This article has been accepted for publication in a future issue of this journal, but has not been fully edited. Content may change prior to final publication. Citation information: DOI 10.1109/TIE.2018.2847652, IEEE Transactions on Industrial Electronics

# Modelling and Control of Magnetic Actuation Systems based on Sensorless Displacement Information

A. Cervera, *Student Member, IEEE,* O. Ezra, A. Kuperman, *Senior Member, IEEE,* and M. M. Peretz, *Member, IEEE*

***Abstract*- The paper reveals design and implementation of a magnetic actuation system (MAS) with non-invasive displacement measurement by current sensing only. Platform-independent MAS modeling methodology is utilized, describing the cross-coupled system behavior by physical representation of mechanical and electromagnetic counterparts. An extended non-linear inductor model is developed, demonstrating the challenging control task of displacement regulation. The inductor model facilitates the development of a combined current sensing methodology employing non-invasive displacement measurement. The combined sensor, based on adding a "shunt inductor" in series to the main actuator, performs both high resolution displacement and dc current measurement with fast response and minimum losses. MAS model and the combined sensor based operation have been experimentally verified on a single-axis levitator prototype.**

*Index Terms*- **MAGLEV, sensorless measurement, modeling.**

## I. Introduction

Magnetic actuation systems (MAS) are used to stabilize contactless floating or rotating systems, replacing ordinary mechanical (passive) counterparts. The non-contact property dramatically reduces the losses and allows operation with higher mechanical speeds. Such systems are used in a variety of applications, e.g. machine-tools (heavy-duty, high-speed, high-precision), flywheels for energy storage, turbo-molecular pumps, turbo-generators, aerospace positioning, magnetic bearings etc. [1]-[5]. Limiting factors preventing MAS from replacing their mechanical precursors are space and maintenance requirements as-well-as complex, and rather costly, electronic control scheme and associated circuitry, required to facilitate high precision displacement control [6]. Sensorless control schemes have also been introduced, exploiting changes in the actuator physical parameters such as flux or inductance, and measured by observing the reaction to an injected high-frequency signal [8-10]. Another obstacle for parameter and position estimation by simple means is the lack of mutual interaction between mechanical, electromagnetics, and electrical engineers to provide an accurate definition and analysis tools for the multidisciplinary problem on-hand, as evident in the differences in the publications of each discipline. The concept of MAS, and AMB in particular, is widely covered in the mechanical engineering literature [7], including several potential solution for power drivers [5]. However, several assumptions and approximations commonly applied result in either poor closed-loop performance, or increased complexity of the end-product. For example, although the electromagnetic actuator is formed based on a magnetic element with a variable gap and bias, its inductance is in many cases assumed as constant, relying on the fact that movement is somewhat limited. This assumption prevents accurate design and prediction of the performance. Another example is that although cross-platform linkage is theoretically available these days, it is evident that in practice each of the units comprising the system (power stage, electromagnet, sensors and controller) is preferably analyzed and designed via a different platform with virtually no link of communication between the designs, which, in turn, adds complexity to the system. A simplistic electromagnetic actuation system typically comprises an open-core inductive actuator that applies attraction force via its flux lines on a ferromagnetic element. The actuator is fed by a current-controlled power driver such that the desired displacement between the actuator and the element is maintained. Precise and efficient sensing of both the dc current and the floating rotor (flotor) displacement are essential in order to achieve a stable high performance system [5], [6].

The main objectives of this study are therefore: 1) facilitating a single platform, generic modeling methodology for MAS applications, applicable to common simulation tools (e.g. Spice, PSIM, Matlab etc.) and is based on the physical representation of the system; 2) introducing an efficient novel combined sensor for both current and displacement detection that uses a minimum components and a simple circuit that outputs two signals proportional to dc current and displacement.

Key contributions of this paper include 1) a simple modeling extension for variable inductors as function of both current and air gap; 2) a magneto-electro-mechanical MAS model for a complete system, including the controller, providing a straightforward platform for system development and design; 3) non-linear actuator representation for magnetic modelling that includes both inductance and current variations effects on the energy; 4) plant model extraction and revalidation of the complex, unstable open-loop characteristics 5) Detailed controller and control scheme design including non-invasive displacement estimation. Finally, simulations and experiments successfully validate the presented findings.

## II. Actuator Modeling

A typical actuator (Fig. 1) consists of an open-core electromagnet, applying attraction force on a ferromagnetic element, named *flotor* [6]. The objective of the MAS system is providing the actuator with energy sufficient for translated attraction force to overcome other auxiliary forces so that the flotor sustains within the desired displacement from the core. The energy required to regulate the flotor position may considerably vary as a function of the desired operating point,

This article has been accepted for publication in a future issue of this journal, but has not been fully edited. Content may change prior to final publication. Citation information: DOI 10.1109/TIE.2018.2847652, IEEE Transactions on Industrial Electronics

i.e. the air-gap. This is due to the fact that the stored energy in the inductor $w_L$ depends on both the inductance $L$ and the drive current $I$. To model this behavior, two cross-coupled behavioral blocks are applied, as shown in Fig. 2, modeling the mechanical impact [8], [9] and inductance behavior.

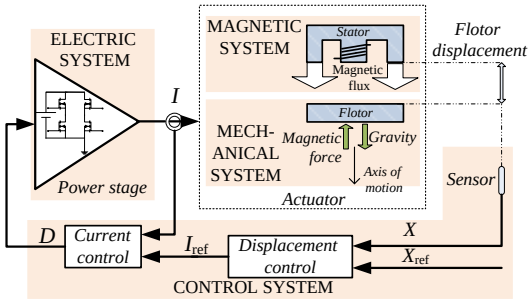


Fig. 1. Conceptual representation of a single-axis MAS, divided into electric, magnetic, mechanical and control subsystems. $X$: flotor displacement; $X_{ref}$: reference flotor displacement; $I_{ref}$: Reference inductor current; $D$: power-stage duty-cycle; $I$: produced inductor current.

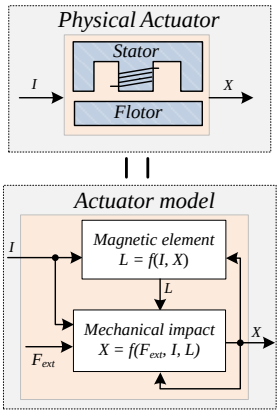


Fig. 2. Electromagnet model with two cross-coupled units: mechanical system and varible inductor. $F_{ext}$: external forces on the flotor

The relationship between the sum of forces to the flotor displacement may be expressed as

$$ma = F_{ext} - F_{mag}\,, \tag{1}$$

where $m$ and $a$ are the mass and acceleration of the flotor respectively, $F_{mag}$ is the magnetic force, and $F_{ext}$ represents external forces such as gravity. $F_{mag}$ is a result of the total energy of the actuator [6], given by

$$F_{mag} = -\frac{dw_L}{dx} = -\frac{d}{dx}\frac{LI^2}{2}\,, \tag{2}$$

where $w_L$ is the magnetic energy. It should be mentioned that $L$ is variable which depends on $X$ and $I$ (see Fig. 2). Assuming gravity as the only external force, the following then holds for a single-axis actuator,

$$a = g - \frac{\frac{d}{dx}w_L}{m}\,, \tag{3}$$

where $g \approx 9.8$ m/s$^2$ is gravity acceleration. Integrating the acceleration over time further gives velocity and displacement $X$. According to (2), the derivative of magnetic energy with respect to the displacement is required to obtain magnetic force. Generally, simulation tools apply time as the varying parameter by default.

To overcome this the following transformation is applied,

$$\frac{d}{dx}w_L = \frac{d}{dt}w_L \Big/ \frac{d}{dt}X\,, \tag{4}$$

which may be implemented using readily available functions, embedded in typical simulators, as shown in Fig 3. To avoid potential convergence problems caused by division by zero, a saturation/limiter element (e.g ETABLE in PSpice) may be applied to the calculation of $dx/dt$. In order to express the inductance as function of displacement and current, an extension to the non-linear inductor model revealed in [10] is utilized. There, a fixed inductor $L_0$ is reflected via a non-linear transformer to model variable inductance $L(K,L_0)$, as shown in Fig. 4, with dependent sources defined by

$$E = \frac{V_L}{K}\,, \quad G = I_{L0}\,, \tag{5}$$

where $E$ and $G$ are the dependent voltage and current sources of the non-linear transformer, and $k$ is the input to vary $L(k)$.

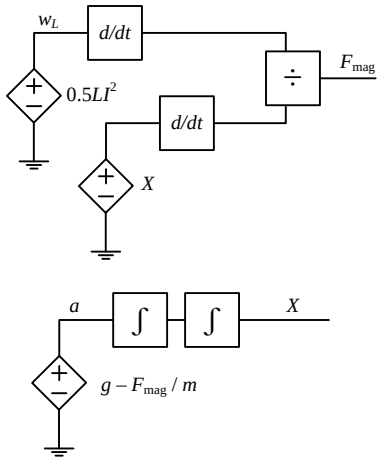


Fig. 3. Force and air-gap calculation.

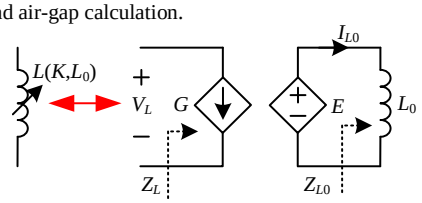


Fig. 4. Non-linear inductor model.

The impedance of $L_0$ i.e. $Z_{L0}$ is reflected to the primary side as

$$Z_L = \frac{KV_{L0}}{I_{L0}} = KZ_{L0}\,, \tag{6}$$

where $Z_L(K,L_0)$ is the variable impedance for $L(K,L_0)$. If $K$ is defined as $K = f(I,X)$, the model then emulates the non-linearity of the device. In a simulator environment, $K$ may be easily defined accordingly.

To facilitate the dependence of the inductance on the displacement and the current, a reluctance model analysis approach is adopted [11]-[13]. Model derivation is demonstrated next for an E-core type actuator, shown in Fig. 5 along with the equivalent reluctance circuit. For a component section of length $l$, cross-section $A$, and permeability $\mu$, the magnetic reluctance $R$ is

$$R = \frac{l}{\mu A}\,. \tag{7}$$

This article has been accepted for publication in a future issue of this journal, but has not been fully edited. Content may change prior to final publication. Citation information: DOI 10.1109/TIE.2018.2847652, IEEE Transactions on Industrial Electronics

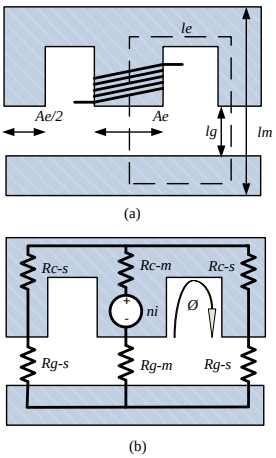


Fig. 5. (a) E-core based actuator structure and dimensions, (b) reluctance model.

TABLE I: RESISTANCES OF E-CORE RELUCTANCE MODEL

| *Section* | *Variable* | *Reluctance* |
|---|---|---|
| *Middle-section core* | $R_{c\text{-}m}$ | $(l_e - l_m)/(\mu_0\mu_r A_e)$ |
| *Side-section core* | $R_{c\text{-}s}$ | $l_m/(0.5\mu_0\mu_r A_e)$ |
| *Middle air-gap* | $R_{g\text{-}m}$ | $L_g/(\mu_0 A_e)$ |
| *Side air-gap* | $R_{g\text{-}s}$ | $L_g/(0.5\mu_0 A_e)$ |

Following (7) and given the core dimension in Fig. 5(a), the reluctance of the air-gap (symbolized as *g*) and the core section reluctance (symbolized as *c*) will be $R_g = l_g/(\mu_g A_g)$ and $R_c = l_c/(\mu_c A_c)$. The following simplifications are made: for air $\mu_g \approx \mu_0$ i.e. vacuum permeability, the air and core effective cross sections are similar and commonly expressed as $A_e$, and $\mu_c$ is expressed in relation to air by a factor $\mu_r$ providing $\mu_c = \mu_0\mu_r$. The equivalent total reluctance $\Sigma R$ is extracted by analyzing the magnetic path shown in Fig. 5 and detailed in Table I.

$$\sum R = R_{g-m} + R_{c-m} + \frac{R_{g-s}}{2} + \frac{R_{c-s}}{2} = \frac{l_e + 2\mu_r l_g}{\mu_0 \mu_r A_e} . \quad (8)$$

The electromagnet magnetomotive-force (MMF) is given by

$$\mathrm{MMF} = nI = \Phi\Sigma R , \quad (9)$$

where *n* is the number of turns and $\Phi$ is the magnetic flux. Applying Faraday's law, the winding voltage may be expressed as

$$V = n\frac{d\Phi}{dt} = \frac{n^2}{\Sigma R}\frac{dI}{dt} = L\frac{dI}{dt} . \quad (10)$$

The inductance *L* is then extracted as

$$L = \frac{n^2}{\Sigma R} \quad , \quad R = f\left(\mu_r, l_g\right) . \quad (11)$$

Combining (8) and (11), the inductance is obtained as

$$L = \frac{n^2 \mu_0 A_e}{l_e}\frac{\mu_r}{1 + 2\mu_r l_g / l_e} \quad , \quad \mu_r = f\left(I\right) , \quad (12)$$

where $l_g$ is the air gap and $\mu_r$ is the permeability. The latter depends on the current and can be obtained from either the manufacturer data [15] or experimentally [10]. An approximation for $\mu_r$ can be obtained by

$$\mu_r \approx \frac{\mu_{ini}}{1 + \left(H / H_{\mathrm{sat}}\right)^j} \quad , \quad H = nI / l_e , \quad (13)$$

where *H* is the magnetic field proportional to *I*, $H_{\mathrm{sat}}$ is the saturation field-magnitude, $\mu_{\mathrm{ini}}$ is the permeability initial value $\mu_{\mathrm{ini}} = \mu_r(I = 0)$, and *j* sets the permeability slope.

The magnetic subpart of the actuator is given by (12), (13) and may be implemented in simulation environment as dependent voltage sources or function blocks. Combination with models in Figs. 3 and 4 creates the full cross-coupled model of the actuator, in which *I* serves as the model input (supplied by the power stage). It should be noted that the effect of hysteresis losses and other non-linarites can be incorporated into the value of $\mu_r$ as described in [10]-[12],[14].

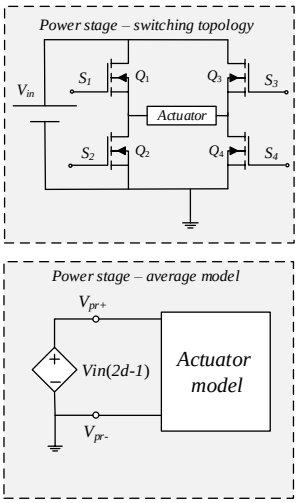


Fig. 6. Power stage and average model for complementary PWM.

MAS power driver is typically realized by a full-bridge circuit, operating in either complementary PWM, phase-shifted, or three-level switching scheme [15]-[17]. The topology allows bi-directional current flow through the actuator, which accelerates the attraction force formation.
Behavioral model approach [18] has been applied to model the driver. Switching-cycle-averaged voltage across the actuator terminals $V_{L,\mathrm{avg.}}$ may be expressed as

$$V_{L,\mathrm{avg.}} = V_{in}\left(2D - 1\right) , \quad (14)$$

where $V_{in}$ is the supply voltage. Assuming complementary PWM operation, the power stage and its behavioral model, which can be implemented in a numerical simulator, is shown in Fig. 6.

It should be noted that methods of back EMF, inductance variation and more can all be applied to interpret the obtained information from a displacement sensor. In this work the displacement information is extracted based on inductance variation since it directly correlates to the modelling methodology and the extraction of the parameters. Back-EMF method is also applicable for closed-loop operation; however it would not directly correlate to the following analysis methods. The information extraction method that is applied in this study, that is, by sensing inductance is the key for both back-EMF and inductance variation. Further details of the sensor realization as well as detailed survey of possible sensing methods can be found in Section IV.

This article has been accepted for publication in a future issue of this journal, but has not been fully edited. Content may change prior to final publication. Citation information: DOI 10.1109/TIE.2018.2847652, IEEE Transactions on Industrial Electronics

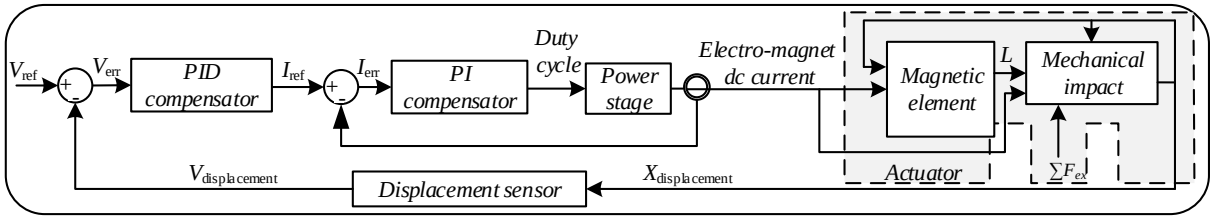


Fig. 7. Control system block diagram

## III. Closed-Loop System

According the aforementioned analysis, the complete MAS model block diagram is constructed as shown in Fig. 7. As can be observed, the magnetic and mechanical variables are a function of the actuator bias current and the flotor displacement. To facilitate a simple controller structure, a two-loop approach is applied, an inner current control loop for the inductor current and an outer control loop for the flotor displacement. The compensation scheme design has been carried out on the basis that open-loop information of the system can be obtained by simulation; therefore, some of the manual derivation burden has been assigned to the simulator. In particular, once an initial current-loop controller has been assigned, the design of the outer loop controller has been carried out solely by simulation.

Based on the power stage model in (14), the inner current loop control-to-output transfer function (power stage plus inductance) can be expressed as

$$\frac{i}{d}(s)=\frac{2V_{in}}{sL} \quad , \quad L=f(I,X) \ , \tag{15}$$

where $i$ and $d$ provide the small-signal values for $I$, $D$ at a specific operating-point. This implies that the dynamics of the system are strongly dependent on the operation point, as the inductance may significantly vary. Fig. 8 shows the control-to-output transfer functions of the inner current loop for several operating conditions (different air-gaps and bias current), as well as the selected compensation type (lag-lead). As can be observed, the compensator has been selected, in this simplistic design, to guaranty the system stability for the entire operation range.

The control-to-output frequency response of the outer displacement loop with the compensation scheme is shown in Fig. 9. It can be observed that the control-to-output transfer function $x/i\,(s)$ consists of 2 real poles, where one of them is located in the right half of the complex plane which implies instability of the system without proper compensation [5], [19]. In this study's extension, the actuators control-to-output transfer function can be expressed as:

$$\frac{x}{i}(s)=\frac{k_i}{s^2m-k_x} \quad , \quad \{k_i,k_x\}=f(I,X) \ , \tag{16}$$

where $k_i$ [N/A] is the force/current factor and $k_s$ [N/m] is the force/displacement factor. As can be seen from (16), the poles of the system are with the same magnitude and differ only by sign, $\lambda_{1,2}=\pm(k_x/m)^{0.5}$. As a result, their influence on the open-loop phase is eliminated in specific frequency and manifests by providing 180° of phase lag throughout the frequency range, as can be seen in Fig. 9. Compensation for such system by linear control tools may be found challenging due to the

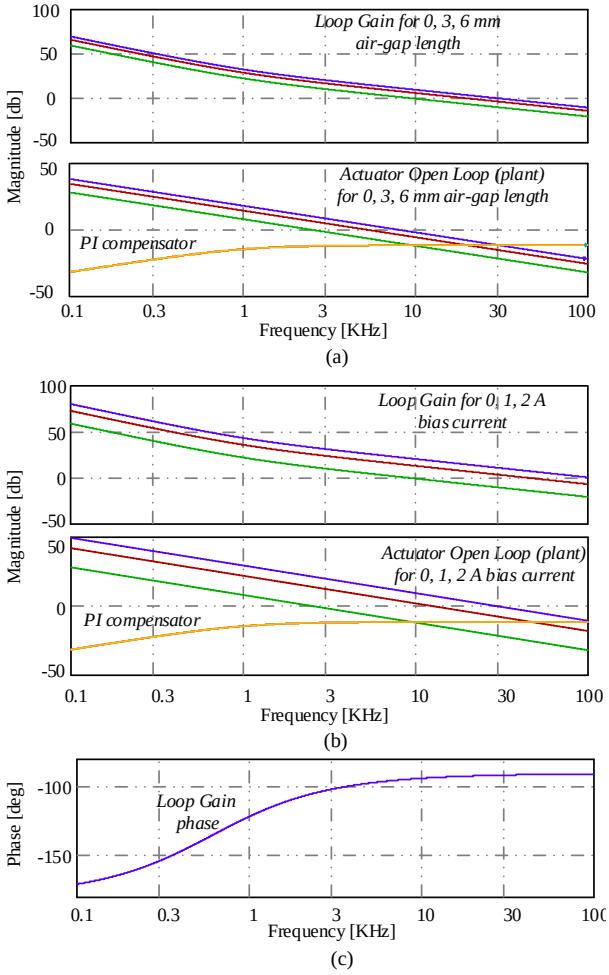


Fig. 8. Magnitude and phase of the inner loop for (a) different air-gap lengths with zero bias current (b) different bias currents with zero air-gap. (c) The loop-gain phase, identical for all cases.

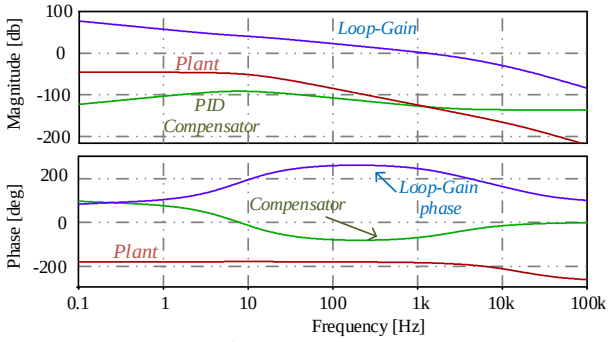


Fig. 9. Magnitude and phase of the outer loop.

This article has been accepted for publication in a future issue of this journal, but has not been fully edited. Content may change prior to final publication. Citation information: DOI 10.1109/TIE.2018.2847652, IEEE Transactions on Industrial Electronics

non-minimum phase behavior of its roots. However, as can be seen in Fig, 10, for the particular frequency range of interest, i.e. beyond the double pole location, the behavior of the system resembles the classical minimum-phase, double pole configuration with 180° phase lag, which can be effectively compensated by a double zero, i.e. PID, compensation scheme. In other words, a derivative part is mandatory to assure stability of the outer loop since some amount of phase lead is required to provide positive phase margin. This approach has been realized in the current study, as can be seen in Fig. 9. It should be noted, and can be observed that, the design of the outer loop is carried out under the assumption that the bandwidth of the inner loop is sufficiently larger that of the outer loop, therefore reducing the complexity of the compensator.

Nevertheless, one must take in to consideration the switching frequency of the power-stage and the ADC sampling rate if digital controller is used [20],[21]. The discrete nature has an effect on the loop-gain and phase near the switching frequency which should be accounted for if the designed bandwidth approaches the sampling or switching-frequency.

## IV. Non-Invasive Current and Displacement Sensor

Traditionally, displacement is measured using physical sensors. The requirements for a displacement sensor are wide frequency response, low noise, compactness and high reliability. There are three common types of displacement sensors that are suitable for MAS applications, capable of sensing within micro-meter range. Optical sensors [6],[22] utilize the basic principle of covering a light source opposite to a photo transistor by the flotor so the sensor output current will be almost linear to the flotor displacement. However, they are sensitive to dirt and oil. In capacitive sensors [5], [6], [23], the sensor and the target are used as two plates of parallel-plated capacitor, and interface circuit transforms the capacitance to displacement signal. The main drawbacks are the need of conductive plate on the target that will be connected to ground or another fixed voltage. Humidity, pressure, dirt and oil can modify the dielectric constant and result in measurement error. Electromagnetic sensors [23], [24] are based on open-core electromagnet with varying inductance, mostly due to eddy currents generation. The target position is sensed by interfacing an inductance detector circuit as e.g. oscillator. Those sensors are contact-free and insensitive to the environment. Popular current sensor for MAS applications is active sensor such as a Hall-effect [22], [25] to obtain the actuator dc current. This leads to large size, higher power consumption and increased complexity of the system. Sense-resistor enables the detection of both dc and ac current [25]. The drawback of sense-resistor is that in addition to the conduction losses, the resistor's stray inductance leads to errors and low SNR. Other solutions use the combination of digital-control with transformer-based current sense circuit to obtain the dc current from the secondary winding waveform [26-27]. These methods add current transformer in series to one of the power stage switches, creating a pulsed waveform with peak current that is proportional to the primary dc value. Such implementation does not exploit the information of the flotor displacement that can be obtained from actuator current ac component and is usually filtered out for a higher SNR measurement of the dc current. In order to gain the full information for sensorless displacement, one study suggested injecting a high-frequency signal to the existing current through the PWM controlling the AMB. This was used to estimate parameters change and provide linear feedback. A more recent work suggested a method to estimate resistance changes in solenoid valves by current sampling only. Further comparison between sense methods can be found in [27], with more information on sensorless displacement found in [28-37].

### A. Principle of operation of the non-invasive sensor

The H-bridge amplifier, shown in Fig. 6, consists of four transistors to allow bi-directional current in the winding [11]. When $S_1$ and $S_4$ are ON, $V_{in}$ is applied to actuator terminals. Alternatively, when $S_2$ and $S_3$ are ON and $-V_{in}$ is applied. Additional operation modes for the circuit are described in detail in [38]. According to Faraday law while neglecting the winding starry resistance, and taking (12) into account, the current change rate and inductance are inversely proportional, that is

$$\left|\frac{dI}{dt}\right| = \frac{V_{in}}{L} = \frac{l_e + 2\mu_r X}{\mu_0 \mu_r A_e n^2} \quad , \quad \begin{matrix} L = f(I,X) \\ \mu_r = f(I) \end{matrix} . \tag{17}$$

Combining (13) and (17) yields

$$\left|\frac{dI}{dt}\right| = \frac{V_{in}}{L_0}\left[1 + \alpha X + \left(\frac{I}{I_{sat}}\right)^j\right] \quad , \quad \alpha = 2\frac{\mu_r}{l_e} , \tag{18}$$

where $L_0$ is the actuator inductance with no air gap and zero current and $I_{sat}$ is the saturation current that matches $H_{sat}$. According to (18), linear relation exists between the current change rate and the displacement. Therefore, flotor position may be obtained by measuring *di/dt* of the actuator.

The sensor topology in its generic form, as described in Fig. 10, requires a sense inductor with significantly smaller inductance than the actuator that will not be saturated in more than the predicted maximum current. This is required to guarantee minimum intervention in the MAS operation.

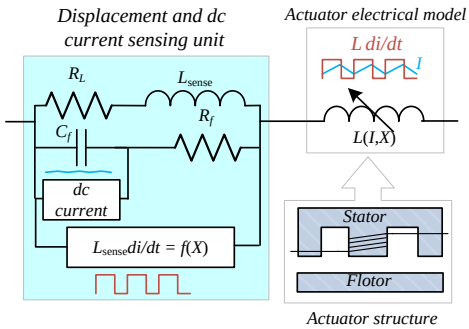


Fig. 10. The non-invasive sensor connected in series to the actuator, represented by a variable inductor.

The reason for adding an additional inductor as a sensing element serves twofold: (a) the measurements are accurately obtained on a fixed inductance, and (b) the dc component can be measured using a simple circuit. Since the same current flows in the sense inductor current, the sense inductor developed voltage is proportional to the actuator's *di/dt*.

This article has been accepted for publication in a future issue of this journal, but has not been fully edited. Content may change prior to final publication. Citation information: DOI 10.1109/TIE.2018.2847652, IEEE Transactions on Industrial Electronics

Hence, if the current is given or significantly smaller than $I_{pole}$, it is linear to the flotor displacement, seen by

$$\left|V_{sense}\right| = L_{sense}\left|\frac{dI}{dt}\right| = KV_{in}\left[1+\alpha X+\left(\frac{I}{I_{sat}}\right)^{j}\right] . \qquad (19)$$

Therefore, given the input voltage and actuator parameters, flotor displacement could be obtained from the sensing inductor voltage. However, if $I/I_{sat}$ is not significantly smaller than unity, dc current should also be taken into account during measurements. In addition, in case a double-loop control structure is utilized to control the MAS, accurate and fast dc current sensing is crucial for the design of both current and displacement control loops.

Since the current flows through a constant inductance, a simple DCR current sensing may be carried out (see Fig. 10) [39]. This technique is based on low pass *RC* network that filters the voltage across the inductor. The voltage across the capacitor is

$$V_{Cf}(s) = \frac{V_{sense}}{1+sR_fC_f} = IR_L\frac{1+s\left(L_{sense}/R_L\right)}{1+sR_fC_f} , \qquad (20)$$

where $R_L$ is the winding stray resistance. If $C_f$ and $R_f$ are selected to ensure that $L_{sense}/R_L = R_fC_f$, then $V_{Cf} = IR_L$ and hence $V_{Cf}$ would be directly proportional to $I$. Since only dc component of the current is required, selecting a larger $C_f$ would filter out the ripple, yet the capacitor voltage will be proportional to the dc current. Obtaining the dc current using the DCR technique, enable to exploit the flotor displacement from the sense inductor current.

Operation of the sensor as part of the MAS is demonstrated in Fig. 11. During steady state #1, actuator inductance remains constant ($L_1$). The converter operates with 50% duty cycle, forcing the current to increase/decrease with the rate of $V_{in}/L_1$, so the average current does not change. The voltage across the sense inductor is as a square wave with amplitude of $L_{sense}(V_{in}/L_1)$. The voltage at the capacitor terminals $V_{Cf}$ is proportional to the dc component of the current (neglecting the small ripple). When the displacement reference is changed, the current changes as well. During the transient, the current induces stronger magnetic force so the flotor position follows the new reference. When the MAS reaches steady state #2, the actuator inductance increases to a new value, $L_2$, leading to a smaller current change rate, $V_{in}/L_2$. The voltage across sense inductor voltage is again a square wave yet with different amplitude, representing displacement change.

### B. *Practical issues*

A key factor to assist the design of accurate and reliable displacement sensor is the consideration of the common-mode voltage at the terminals of the sense inductor and the filter capacitor. Instrumentation amplifiers with higher CMRR are required to overcome this issue. Since the magnitude of the voltage at the sensing unit terminals is $V_{in}$, which might be beyond the absolute maximum rating of the instrumentation amps, and in order to reduce the common-mode interference, a voltage divider is added to obtain a lower voltage measurement referenced to ground. In addition, protection clamps should be used to cut off switching noise spikes, as shown in Fig. 12. An outcome of adding voltage dividers is dc offset error at the dc signal amplifier negative terminal. This is due to the current flowing path from $R_f$ to ground. The dc error can be attenuated by selecting significantly larger resistors for the voltage dividers than the filter resistor ($R_{d1}$,$R_{d2}$ >> $R_f$). Another approach is by using amplifier with reference pin. The output voltage of amplifier such as AD8428 is developed with respect to the potential at the reference terminal, so dc signal may be calibrated.

Another practical issue that should be taken into account is the influence of the sense inductor on the current change rate, *di/dt*. In case the sense inductance is significantly smaller than the actuator inductance, input voltage $V_{in}$ is fully applied on the actuator. However, actuator and sense inductances effectively create an inductance voltage divider, i.e. the voltage across the sense inductor is actually given by

$$V`_{sense} = L_{sense}\frac{V_{in}}{L+L_{sense}} \quad , \quad L = f\left(I,X\right) . \qquad (21)$$

Measurement error for $I < I_{sat}$ is then given by

$$V_{error} \approx KV_{in} - V`_{sense} = V_{in}\frac{L_{sense}^2}{L\left(L+L_{sense}\right)} . \qquad (22)$$

Therefore, minimum actuator inductance should remain much larger than $L_{sense}$ to reduce measurement error.

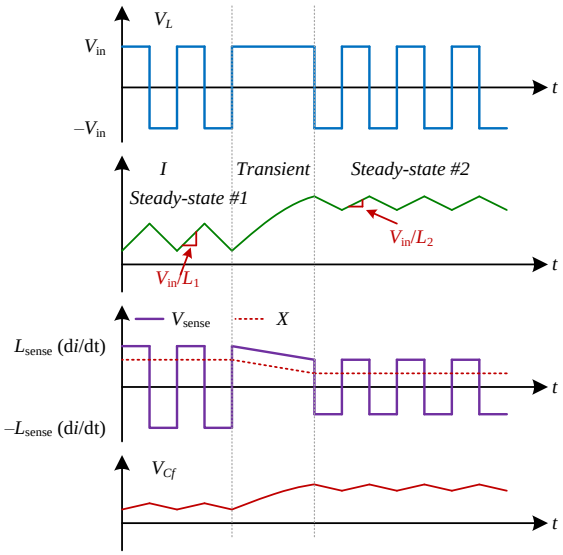


Fig. 11. Power stage and the sensor waveforms during steady state and transients.

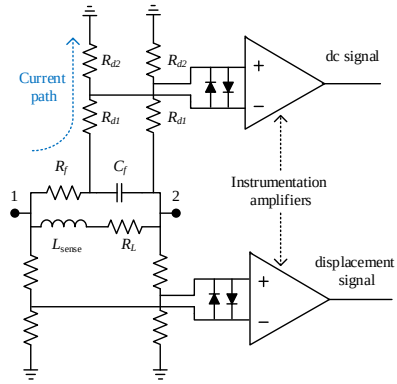


Fig. 12. Practical implementation of the sensor, consist of voltage dividers and clamping diodes.

This article has been accepted for publication in a future issue of this journal, but has not been fully edited. Content may change prior to final publication. Citation information: DOI 10.1109/TIE.2018.2847652, IEEE Transactions on Industrial Electronics

## V. VERIFICATION

In order to demonstrate the combined current and non-invasive displacement sensor, simulation and experimental setups were established. The electro-magnet and the power stage parameters are summarized in Table II.

### A. Simulations

Simulation setup (SPICE software) consisted of an H-bridge power stage and actuator realization model described by Figs. 3, 4, and 7. Two simulations were carried out for demonstration of current and displacement sensing. Fig. 13 presents the results of displacement measurement simulation. Trapezoid wave represents the flotor position and serves as the input to the inductance calculation block. As can be noticed, flotor displacement variations change the actuator inductance. The simulation verifies linear relation between the output amplitude, which amplifies the sensed voltage by a factor of 40, and flotor displacement.

TABLE II: VERIFICATION SETUP PARAMETERS

| ***Electro-magnet parameters*** | | |
|---|---|---|
| ***Parameter*** | ***Symbol*** | ***Value*** |
| Core material | | 3F3 |
| Effective length | $l_e$ | 130 mm |
| Effective area | $A_e$ | 540 mm$^2$ |
| Winding number | n | 100 |
| ***Displacement and current sensor*** | | |
| ***Parameter*** | ***Symbol*** | ***Value/Model*** |
| Input voltage | $V_{in}$ | 20 V |
| Frequency | $f_{sw}$ | 100 kHz |
| Micro-controller | | dsPIC33fj15gs502 |
| Voltage dividers | | 16.5 kΩ, 150 kΩ |
| Filter capacitor | $C_f$ | 10 uF 0805 |
| Filter resistor | $R_f$ | 500 Ω 0805 |
| Clamping diodes | | 1SS384 |
| Instrumentation amplifiers | | AD8428 |
| Boot-strap drivers | | ISL6700 |
| H-bridge transistors | $S_1$-$S_4$ | Si4190ADY |

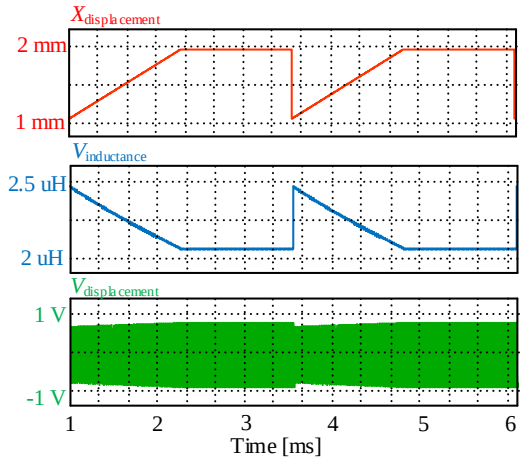


Fig. 13. Flotor displacement, actuator inductance and displacement sensor output voltage (envelope) upon independent trapezoidal shaped displacement change.

Fig. 14 demonstrates actuator current and filter capacitor voltage (multiplied by 100 without offset calibration) upon duty cycle variation from 60% to 40%. Apparently, DC current sensor 70mV/1A resolution measurements.

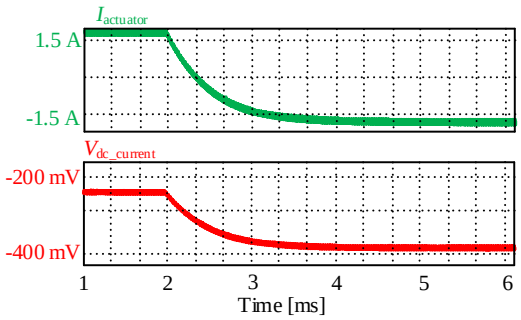


Fig. 14. DC current sensor output voltage compared to the actuator current.

In order to validate the whole MAS model, as well as the displacement sensing in closed-loop, simulation results were obtained for both the inner and outer loop operation. Fig. 15 presents the step response to a change in the displacement reference and the system (and model) reaction in both the actual displacement signal and actuator current.

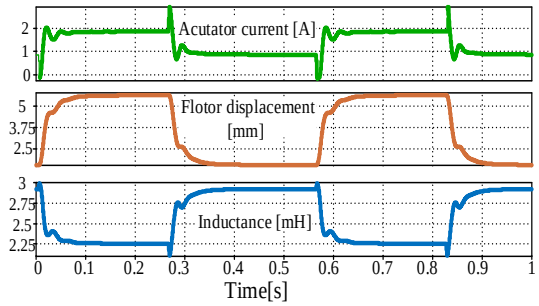


Fig. 15. Actuator current, displacement and inductance obtained by simulation in response to a step in the displacement reference.

### B. Experiments

To validate the MAS model using the combined sensor concept, expression (12) derived based on theoretical analysis and manufacturer data has been compared with several experimental inductance curves as a function of the current [13], for several air-gap settings (15 µm, 100 µm, 130 µm). The actuator parameters were $l_e$ = 68 mm, $A_e$ = 69 mm$^2$, $n$ = 17, $H_{pole}$ = 30 A/m, j = 1.5757, $\mu_{ini}$ = 3000. The results are summarized in Fig. 16. Good matching is evident.

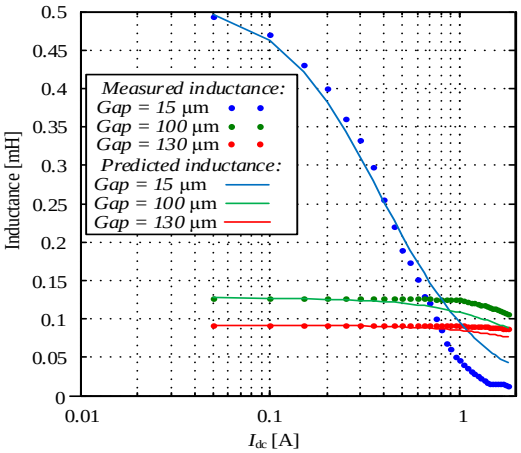


Fig. 16. Experimental results and the model simulation results.

This article has been accepted for publication in a future issue of this journal, but has not been fully edited. Content may change prior to final publication. Citation information: DOI 10.1109/TIE.2018.2847652, IEEE Transactions on Industrial Electronics

Then, an experimental setup comprising the power stage and actuator was built, as shown in Fig. 17 in which the drive stage, input capacitors, sensor voltage dividers etc. were omitted for simplicity. The prototype is pictured in Fig. 18. The controller has been implemented digitally on a microcontroller platform (dsPIC33FJ16GS502) which includes an internal ADC, with sampling synced to the PWM output. The actuator was constructed by half-E-core while an I-core element was used for the flotor. Core magnetic parameters as well as power stage and sensors parameters matched the ones in Table II. The controller coefficients have been extracted based on a modified Ragazinni method [19] in similar to [40,41].

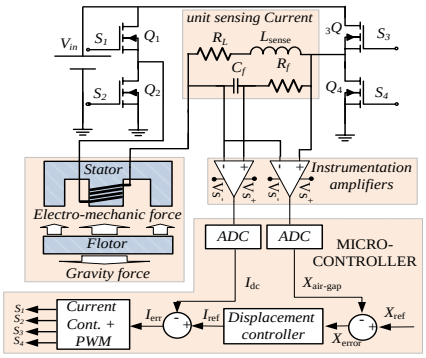


Fig. 17. Experimental setup schematic.

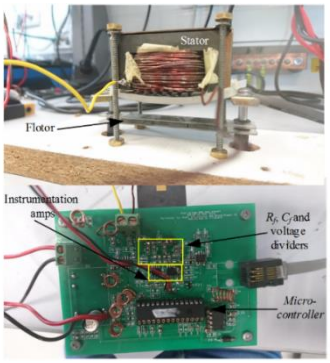


Fig. 18. Actuator prototype pictured. The power stage is located on the buttom side of the PCB.

Fig. 19 presents the output of the DC current sensor compare to measurements taken by an external active sensor, validating the proposed sensor current proportionality to the actuator dc current in steady-state operation and during a transient. The experiment was carried out by closing the inner loop only, i.e. the dc current references were manually set to validate the inner closed-loop design.

To validate the performance of the displacement sensor, air-gaps between 0.05-1 cm have been set in open-loop manner first. The results are shown in Fig. 20, presenting the displacement sensor output (blue) and the current obtained by an external active current sensor (green). The sample and hold signal (red) shows that A/D samples the signals when no noise is present. In this experimental setup, at the sensing range mentioned, the measurement sensitivity is found to be 25 mV/mm minimum. Fig. 21 presents the step response to a change in the displacement reference and the system reaction in both the actual displacement signal and actuator current. A very good agreement with the simulation (cf. Fig. 15) may be observed, validating the model prediction capability and controller design.

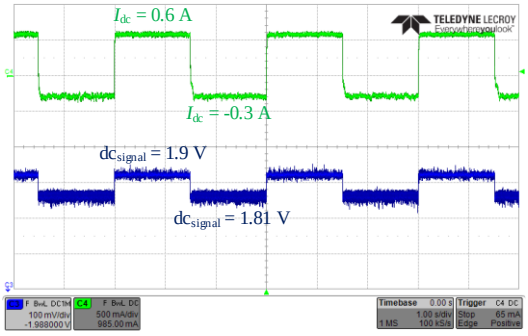


(a)

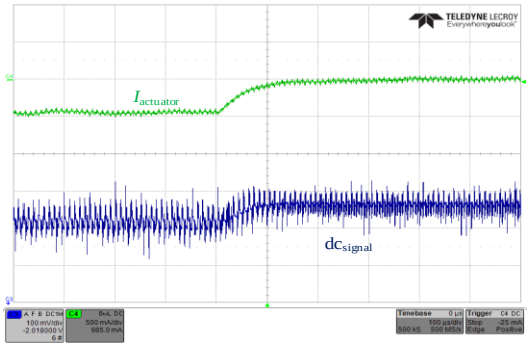


(b)

Fig. 19. Experimental results of the actuator's current by Hall-effect external sensor and the DCR current sensor for: (a) steady performances (1 sec/div) and (b) dynamic performances (100 $\mu$sec/dev).

## VI. Conclusion

In this paper, a novel sensor for displacement and current for multidisciplinary MAGLEV applications such as MAS has been developed and verified by simulations and experiments. Association between current change rate, power stage structure, variations of inductance due to the displacement and the inductor geometry were exploited as the foundation to the sensing technic and explained by the relevant mathematical expressions. The proposed sensing technique has a number of advantages: no dependence on the environment, simple calibration and design, high linearity, small volume, fast response, small power losses and low price. The established sensing technic may be applied to MAGLEV application and to any other power circuits consisting inductive component and require current measurement.

## References

[1] B. Bolund, H. Bernhoff, M. Leijon, "Flywheel energy and power storage systems," *Renew. Sust. Energy. Rev.*, vol. 11, no. 2, pp. 235-258, 2007.

[2] M. Subkhan, M. Komori, "New concept for flywheel energy storage system using SMB and PMB," *IEEE Trans. Appl. Supercond*, vol. 21, no. 3, pp. 1485–1488, June 2011.

[3] S. Kusagawa, J. Baba, K. Shutoh, E. Masada, "Multipurpose design optimization of EMS-type magnetically levitated vehicle based on genetic algorithm," *Applied Superconductivity, IEEE Transactions on*, vol.14, no.2, pp.1922-1925, June 2004.

This article has been accepted for publication in a future issue of this journal, but has not been fully edited. Content may change prior to final publication. Citation information: DOI 10.1109/TIE.2018.2847652, IEEE Transactions on Industrial Electronics

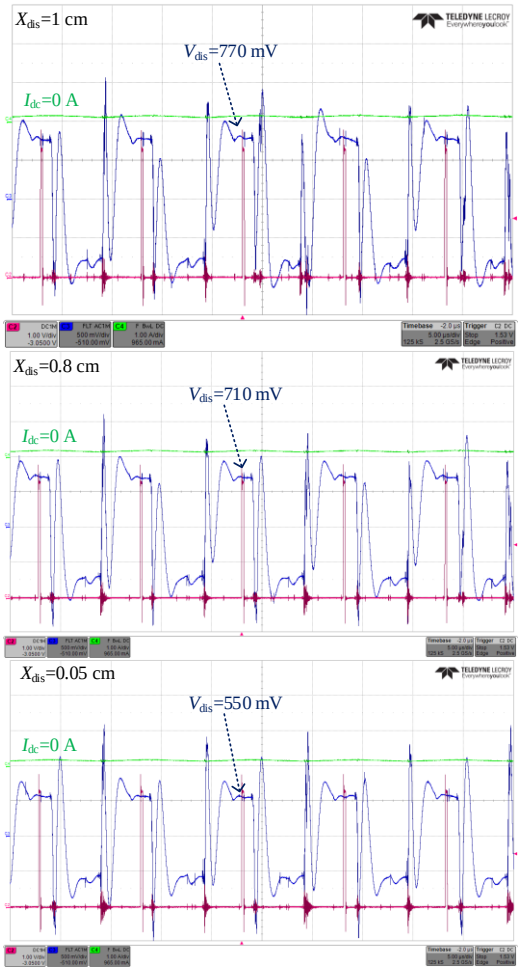


Fig. 20. The non-invasive displacement sensor output for three different air-gaps. A/D sample and hold interrupt is represented by the red signal. $I_{DC}$ (Green, 1A/div), $V_{dis}$ (Blue, 0.5V/div), 5 us/div.

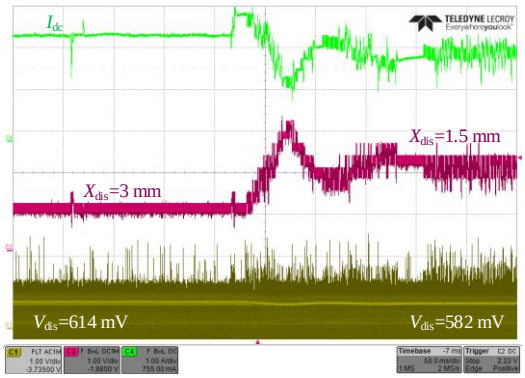


Fig. 21. Actuator current and displacement as measured by The yellow (bottom) signal shows the output of the displacement sensor while the red curve is generated by the micro-controller's D/A to signify the sampled values.


[4] R. Crane, "Magnetic bearings for high speed turbo molecular pumps," in Proc. IEE Colloquium on High Speed Bearings for Electrical Machines, vol. 4, pp. 1-6, April 1997.

[5] A. Chiba, T. Fukao, O. Ichikawa, M. Oshima, M. Takemoto, D. Dorrell, *Magnetic Bearings and Bearingless Drives*, Newnes, Oxford, 2005.

[6] G. Schweitzer, E. Maslen (eds.) *Magnetic bearings: theory, design, and application to rotating machinery*. Springer Verlag, Berlin, 2009.

[7] Y. Hung, N. G. Albritton, F. Xia, "Nonlinear control of a magnetic bearing system," *Mechatronics*, vol. 13, no. 6, pp. 621 – 637, 2003.

[8] J. D. Hewlett, B. M. Wilamowski, "SPICE as a Fast and Stable Tool for Simulating a Wide Range of Dynamic Systems," *International Journal of Engineering Education* 27(2), pp. 217-224, 2011.

[9] H. Toshiyoshi, "A Spice-based multi-physics simulation technique for integrated MEMS," *International Conference on Simulation of Semiconductor Processes and Devices* 2011.

[10] S. Ben-Yaakov, M. M. Peretz, "Simulation bits: a SPICE behavioral model of non-linear inductors," *IEEE Power Electronics Society Newsletter, Fourth Quarter*, pp. 9-10, 2003.

[11] R.W. Erickson, D. Maksimovic, "A multiple-winding magnetics model having directly measurable parameters," *IEEE PESC*, 1998.

[12] D. Medini, S. Ben-Yaakov, "A current-controlled variable-inductor for high frequency resonant power circuits," *IEEE Applied Power Electronics Conference and Exposition Conference Proceedings*, 1994.

[13] J. D. Pollok, W. Lundquist, C. R. Sullivan, "Predicting inductance roll-off with DC excitations," *Proc. Energy Convers. Congress Expo*, pp. 2139–2145, Sep. 2011.

[14] Ferroxcube material specification data sheet, Available at: http://www.ferroxcube.com

[15] Z. Changsheng, C. Yang, Z. Dan, C. Liang, "A current-control mode three-level PWM switching power amplifier for active magnetic bearings," *ICEMS, International Conference on*, pp. 2217-2220, 2008.

[16] Z. Changsheng and M. Zhiwei, "A PWM Based Switching Power Amplifier for Active Magnetic Bearings," *Proc. of 8th International Conference on Electrical Machines and Systems*, Nanjing. China, pp. 1563-1568, 2005.

[17] J. Wang, L. Xu, "Analysis and modeling of a switching power amplifier for magnetic bearing," *IEEE Industrial Electronics and Applications*, 4th IEEE Conference on, 2009.

[18] S. Ben-Yaakov, "Average simulation of PWM converters by direct implementation of behavioral Relationships," *IEEE Applied Power Electronics Conference*, pp. 510-516, 1993.

[19] G. F. Franklin, J. D. Powell, and M. L. Workman, *Digital Control of Dynamic Systems*, 3rd ed. Englewood Cliffs, NJ: Prentice-Hall, 1998.

[20] L. Corradini, D. Maksimović, P. Mattavelli, and R. Zane. *Digital control of high-frequency switched-mode power converters*. Vol. 48. John Wiley & Sons, 2015.

[21] A. Prodic, D. Maksimovic, and R. W. Erickson. "Design and implementation of a digital PWM controller for a high-frequency switching DC-DC power converter." In *Industrial Electronics Society, 2001. IECON'01. The 27th Annual Conference of the IEEE*, vol. 2, pp. 893-898. IEEE, 2001.

[22] P. Ripka and A. Tipek, *Modern Sensors Handbook*. Wiley-ISTE, 2007.

[23] S.Nihtianov, "Measuring in the subnanometer range: capacitive and eddy current nanodisplacement sensors," *Industrial Electronics Magazine, IEEE* , vol.8, no.1, pp.6-15, 2014

[24] Y. Tuo, Y. Yating, D. pingan, L. Yongchun, "The development of displacement eddy current sensor independent of sample electromagnetic properties," *Mechanical and Electrical Technology (ICMET), 2010 2nd International Conference on*, pp.453-457, September 2010.

[25] B. Mammano, "Current sensing solutions for power supply designer," in *Proc. Unitrode Power Supply Seminar SEM-1200*, 1997.

[26] S. Ziegler, L. Borle, and H. H. C. Lu, "Transformer based dc current sensor for digitally controlled power supplies," in *AUPEC*, 2007.

[27] T. Ben-Moha, S. Basovich, M.M. Peretz, S. Arogeti, Z.Brand, "Digitally controlled switch-mode power driver for active magnetic bearings" *Energy Conversion* Congress *and Exposition (ECCE), 2014 IEEE*, pp.3030-3035, September 2014.

[28] Chen HM. Design and Analysis of a Sensorless Magnetic Damper. ASME. *J. Eng. Gas Turbines Power*. 1997;119(1):174-177

[29] Yutaka Kurita, Displacement-Sensorless Control Using Electromagnets : Vibration Control by Current and Magnetic Flux Feedback, JSME international journal. Ser. C, Dynamics, control, robotics, design and manufacturing, Released February 18, 2008

[30] A. L. Dean, M. S. Giusto, "Sensorless measurement of electromagnetic actuator displacement device," US patent US5841621A, 1998

[31] K. K. Sivadasan, "Analysis of self-sensing active magnetic bearings working on inductance measurement principle," in *IEEE Transactions on Magnetics*, vol. 32, no. 2, pp. 329-334, Mar 1996.
[32] T. Mizuno, K. Araki and H. Bleuler, "Stability analysis of self-sensing magnetic bearing controllers," in *IEEE Transactions on Control Systems Technology*, vol. 4, no. 5, pp. 572-579, Sep 1996.
[33] Lichuan Li, T. Shinshi and A. Shimokohbe, "State feedback control for active magnetic bearings based on current change rate alone," in *IEEE Transactions on Magnetics*, vol. 40, no. 6, pp. 3512-3517, Nov. 2004.
[34] P. Garcia, J. M. Guerrero, F. Briz and D. D. Reigosa, "Sensorless Control of Three-Pole Active Magnetic Bearings Using Saliency-Tracking-Based Methods," in *IEEE Transactions on Industry Applications*, vol. 46, no. 4, pp. 1476-1484, July-Aug. 2010.
[35] A. Looser and J. W. Kolar, "An Active Magnetic Damper Concept for Stabilization of Gas Bearings in High-Speed Permanent-Magnet Machines," in *IEEE Transactions on Industrial Electronics*, vol. 61, no. 6, pp. 3089-3098, June 2014.
[36] M. F. Rahman, N. C. Cheung and Khiang Wee Lim, "Position estimation in solenoid actuators," in *IEEE Transactions on Industry Applications*, vol. 32, no. 3, pp. 552-559, May/Jun 1996.
[37] I. Dülk and T. Kovácsházy, "Parameter Estimation in Linear Electromagnetic Devices," in *IEEE Transactions on Industrial Electronics*, vol. 62, no. 6, pp. 3619-3628, June 2015.
[38] D. Wang, F. Wang, Y. Zhao, "Study on three-level power amplifier of magnetic bearings for high speed machine," *Computer Science and Information Technology (ICCSIT), 3rd IEEE International Conference*, pp. 607-612, July 2010.
[39] H. P. Forghani-zadeh, G. A. Rincon-Mora, "Current-sensing techniques for DC–DC converters," *in Proc. IEEE Midwest Symposium. Circuits and Systems*, vol. 2, pp. 577–580, Aug 2002
[40] B. Miao, R. Zane, D. Maksimovic, "Automated digital controller design for switching converters". Proc. IEEE Power Electronics Specialists Conf., PESC-2005, Recife, 2005, pp. 2729–2735
[41] M. M. Peretz and S. Ben-Yaakov, "Time-domain design of digital compensators for PWM DC-DC converters", *IEEE Trans. on Power Electronics*. Vol. 27, No. 1, 284 - 293, 2012.

Alon Cervera (S'12) was born in London, U.K., in 1985. He received the B.Sc. and M.Sc. degrees in electrical and computer engineering from the Ben-Gurion University of the Negev, Beer-Sheva, Israel, in 2011 and 2013, respectively, where he is currently working toward the Ph.D. degree in electrical and computer engineering. His research interests include switched-capacitor converters, voltage regulation techniques, envelope tracking, renewable energy systems, and digital control.

Ofer Ezra was born in Beer-Sheva, Israel, in 1986. He received the B.Sc. and M.Sc. degrees in electrical and computer engineering in 2014 and 2016, respectively, from the Ben-Gurion University of the Negev, Beer-Sheva. He is currently with SolarEdge Technologies Failure Analysis team. His interests include digital control, magnetic components modeling, renewable energy and design for reliability.

Alon Kuperman (M'07-SM'14) received the Ph.D. degree in Electrical and Computer Engineering from Ben-Gurion University of the Negev, Israel, in 2006 while being with Imperial College London as a Marie Curie Training Site Member. He was a Honorary Research Fellow with the University of Liverpool in 2008-2009. He is currently with the Department of Electrical and Computer Engineering, Ben-Gurion University, where he is heading the Power and Energy Systems track. His research interests include all aspects of energy conversion and applied control.

Mor Mordechai Peretz (S'05–M'12) was born in Beer-Sheva, Israel, in 1979. He received the B.Tech. degree in electrical engineering from the Negev Academic College of Engineering, Israel, in 2003, and the M.Sc. and Ph.D. degrees in electrical and computer engineering from the Ben-Gurion University, Negev, Israel, in 2005 and 2010, respectively. From 2010 to 2012, he was a Postdoctoral Fellow in the Laboratory for Power Management and Integrated SMPS, University of Toronto, Toronto, ON, Canada. In 2012, he joined the Department of Electrical and Computer Engineering, Ben-Gurion University, where he is currently the Director of the Center for Power Electronics and Mixed-Signal IC. His research interests include digital and smart control methods for efficient energy processing, switch-mode power supply (SMPS) miniaturization, mixed-signal IC design of SMPS, modeling and computer-aided design, applications of nonlinear magnetics, and renewable energy systems. Dr. Peretz serves as an Associate Editor for the IEEE Transactions on Power Electronics and the IEEE Journal of Emerging and Selected Topics in Power Electronics.